placed by a needle having a small but finite thickness. However, this introduces the possibility of flow separation. If the inclination of the body in the neighborhood of the axis of symmetry is sufficiently small and the Reynolds number sufficiently large, the region where the flow separates is presumably small with respect to the over-all body size. Hence, the changes in the distribution of the pressure coefficient and the skin-friction coefficient are small with respect to those assumed here, so that the results of this paper are essentially correct. On the other hand, if the inclination of the body near the axis of symmetry is sufficiently large and the Reynolds number sufficiently small, the extent of the separated region becomes such that the flow pattern assumed in the theory is unrealistic.

## References

[1] Kennet, H., "The effect of skin friction on optimum minimum-drag shapes in hypersonic flow," J. Aerospace Sci. **29**, 1486–1487 (1962).

[2] Toomre, A., "Zero-lift minimum drag hypersonic bodies," Grumman Aircraft Engineering Corp., Res. Rept. RE-110 (1959).

[3] Miele, A. and Hull, D. G., "Slender bodies of revolution having minimum total drag at hypersonic speeds," Boeing Scientific Research Labs., Flight Sciences Lab. TR 70 (1963).

[4] Miele, A. and Pritchard, R. E., "Slender two-dimensional bodies having minimum total drag at hypersonic speeds," Boeing Scientific Research Labs., Flight Sciences Lab. TR 71 (1963).

[5] Miele, A., "Optimum slender bodies of revolution in Newtonian flow," Boeing Scientific Research Labs., Flight Sciences Lab. TR 56 (1962).

[6] Miele, A., "The calculus of variations in applied aerodynamics and flight mechanics," Boeing Scientific Research Labs., Flight Sciences Lab. TR 41 (1961).

[7] Miele, A. (ed.), *Extremal Problems in Aerodynamics* (Academic Press, New York, 1964).

[8] Miele, A. and Cole, J., "A study of optimums lender bodies in hypersonic flow with a variable friction coefficient," Boeing Scientific Research Labs., Flight Sciences Lab. TR 66 (1963).

## General Bibliography

Chapman, D. R., "Airfoil profiles for minimum pressure drag at supersonic velocities. General analysis with application to linearized supersonic flow," NACA TR 1063 (1952).

Chapman, D. R., "Airfoil profiles for minimum pressure drag at supersonic velocities. Application of shock-expansion theory, including consideration of hypersonic range," NACA TN 2787 (1952).

Eggers, A. J., Resnikoff, M. M., and Dennis, D. H., "Bodies of revolution having minimum drag at high supersonic airspeeds," NACA TR 1306 (1957).

Donaldson, C. D. and Gray, K. E., "Optimization of airfoils for hypersonic flight," Aerospace Eng. **20**, 18–62 (1961).

OCTOBER 1963 AIAA JOURNAL VOL. 1, NO. 10

# Electrical Resistance and Sheath Potential Associated with a Cold Electrode

DONALD L. TURCOTTE* AND JAMES GILLESPIE†
*Cornell University, Ithaca, N. Y.*

**The boundary-layer resistance and the difference in sheath potentials between a pair of electrodes have been measured in a shock tube. Using a small, square electrode and a strip electrode flush with the wall of the shock tube, the electric current that could be drawn across the shock tube was measured as a function of the shock wave position for several applied voltages and load resistances. All measurements were made in air at a shock speed of 4.35 mm/$\mu$ sec and an initial pressure of 1 mm Hg. In the range of applied voltages considered, the boundary-layer resistance was not a function of the current level. The change in the sheath potential was of the order of several volts. A continuum theory is developed to predict the boundary-layer resistance for small current levels and the sheath potential. The sheath solution is separated from the convective compressible boundary-layer problem where ambipolar diffusion dominates. In the sheath, the transport equations for ions and electrons in an electric field are solved numerically. Resulting integrals for the dimensionless boundary-layer resistance and sheath potential are evaluated, both in the sheath and in the compressible boundary layer, to obtain results that can be compared with experiment. Values of the resistance obtained, assuming the ionization reaction to be frozen, are not in agreement with experiment. Reasonable agreement between theory and experiment is obtained for the magnitude of the sheath potential.**

## I. Introduction

THE conduction and diffusion of charged particles to a cold electrode are of considerable current interest. One of the important techniques in plasma diagnostics is the use of probes. In order to interpret probe measurements, it is necessary to understand the effect of the cooled region adjacent to the probe. Also, in magnetohydrodynamic devices such as accelerators and generators, an understanding of the electrical losses associated with cold electrodes is of fundamental importance. Sheath studies are also applicable to re-entry problems. At high re-entry velocities considerable ionization occurs. As a result, electrical effects in the boundary layer on the cool re-entry body can have a considerable effect on heat transfer. To obtain a better under-

Presented at the ARS 17th Annual Meeting and Space Flight Exposition, Los Angeles, Calif., November 13–18, 1962; revision received June 3, 1963. This work was supported in part by Therm Advanced Research of Ithaca, N. Y., under a research grant, and in part by the Air Force Office of Scientific Research under Contract AF 49(638)-544. The authors acknowledge the help of Stanley Howard in developing a theory.

* Associate Professor, Graduate School of Aerospace Engineering. Member AIAA.

† Research Assistant, Graduate School of Aerospace Engineering.

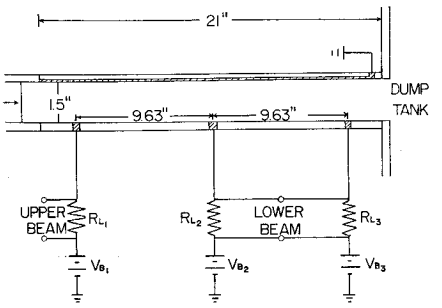


**Fig. 1 Schematic diagram of the shock tube test section and the associated circuits.**

standing of electrical conduction near a cold wall at high gas densities, a combined experimental and theoretical investigation has been undertaken. Some of the results are reported here.

Probably the best way to obtain a plasma that is in thermal equilibrium is by means of a shock wave. Unfortunately, pressure-driven shock tubes are not capable of giving sufficiently high temperatures to produce high-conductivity plasmas. However, sufficient ionization is produced to study conduction phenomena. If electrodes are mounted flush with the walls of a shock tube, a current can be drawn between them which must cross the cold boundary layers that build up on the walls of the shock tube after the incident shock wave passes. The amount of current drawn depends on the resistance of the boundary layers.

The first investigation of electrical conduction in a shock-tube boundary layer was carried out by Brogan.[1] A long electrode was used, and the integrated conduction was measured as a function of the incident shock Mach number. Other experimental investigations of the electrical conduction in a shock-tube boundary layer have been carried out by Pain and Smy[2] and by George and Messerle.[3] In both of these investigations, the current levels were so high that nonequilibrium effects in the boundary layer dominated, and the boundary-layer resistance was low. A theoretical investigation of the problem has been carried out by Jukes,[4] who extended methods used in discharge tubes to the boundary-layer problem.

In the present investigation, small electrodes are used which are capable of determining the local value of the boundary-layer resistance and the difference in the sheath potential between the pair of electrodes. However, the dimensions of the electrodes are large compared with the boundary-layer thickness, so that the path of the electric current through the boundary layer is one-dimensional. The currents drawn are sufficiently small so that the boundary-layer resistance is independent of current level. A theory is developed which predicts values for both the boundary-layer resistance and the sheath potential.

## II. Experimental Results

A standard pressure-driven circular shock tube was used to obtain a slightly ionized plasma. All measurements were made at an incident shock velocity of 4.35 mm/$\mu$sec in air with an initial pressure of 1 mm Hg. The degree of ionization behind the incident shock was approximately 0.5 $\times$ $10^{-4}$. The driver gas was hydrogen. The driven section of the shock tube was a 7-ft length of Pyrex tubing with an inside diameter of $1\frac{1}{2}$ in. The circular test section, 21 in. in length, was attached to the end of the glass tubing. A dump tank, separated from the driver section by a cellophane diaphram, was used to prevent reflected waves.

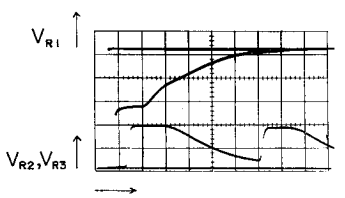


**Fig. 2 Typical oscillogram taken under the conditions $V_{B1} = -6$v, $V_{B2} = V_{B3} = 20$v, $R_{L1} = 100$k$\Omega$., $R_{L2} = R_{L3} = 1$M$\Omega$, $P_0 = 1$mm Hg, $u_s = 4.30$ mm/$\mu$sec, $T_0 = 298$°K. Oscilloscope scales, beam I, 2 v/cm, 20$\mu$sec/cm; beam II, 10 v/cm, 10$\mu$sec/cm.**

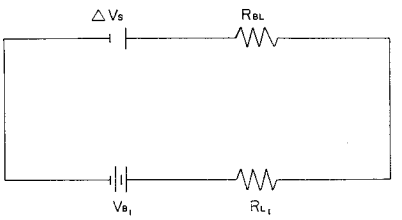


**Fig. 3 Equivalent circuit including the sheath potential difference $\Delta V_s$, boundary-layer resistance $R_{BL}$, battery voltage $V_{B1}$, and load resistance $R_{L1}$.**

Three $\frac{1}{4}$-in. square copper electrodes were mounted 9.63 in. apart, flush with the wall of the Lucite test section. In order to maintain reproducibility, it was necessary to clean the electrodes periodically. Opposite the three square electrodes, a copper strip electrode, $\frac{3}{8}$-in. wide, ran the entire length of the test section. The strip electrode was grounded, whereas the square electrodes were biased. The test section is illustrated in Fig. 1. Also shown are the circuits that allowed each square electrode to be biased. The first electrode was used for all resistance measurements, and the voltage drop across the load resistor was monitored on the upper beam of a Tektronix 555 dual-beam oscilloscope. The second and third electrodes were monitored on the lower beam of the oscilloscope, and the onset of the signals was used to determine the shock velocity.

The experiment was designed so that the current path was through the boundary layer adjacent to the square electrode, through the plasma, and to the strip electrode through the thin boundary layer immediately behind the incident shock wave. Since the voltage drops across the plasma and through the boundary layer into the strip electrode were small compared to the voltage drop across the boundary layer adjacent to the square electrode, they could be neglected.

A typical oscillogram is shown in Fig. 2. Immediately after the incident shock wave passed the first electrode, the measured signal was approximately equal to the applied voltage. The boundary-layer resistance was small compared with the load resistance. After the shock proceeded some distance down the tube, the resistance of the boundary layer $R_{BL}$ was of the same order as the load resistor $R_L$, and the measured voltage decreased. The equivalent circuit is shown in Fig. 3.

In Fig. 4, the voltage drop across the load resistance is plotted against the distance behind the incident shock for bias voltages of 6.0, 3.0, 1.5, $-1.5$, $-3.0$, and $-6.0$ v. All runs were at a shock velocity of 4.35 mm/$\mu$sec with a load resistance of 100 k$\Omega$. Two observations can be made on Fig. 4. First, the boundary-layer resistance appears to be independent of the applied voltage. Second, the voltage

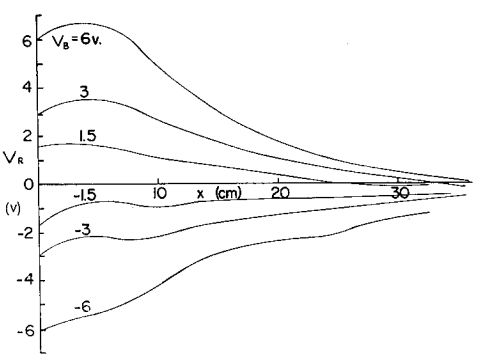


**Fig. 4 Voltage drop across the load resistor as a function of the distance behind the shock wave for several battery voltages; $R_L = 100$ k$\Omega$, $P_0 = 1$ mm Hg, $u_s = 4.35$ mm/$\mu$sec, $T_0 = 298$°K.**

curves all increase as though an additional battery were in the circuit whose strength is a function of the distance behind the incident shock. This shift is attributed to the difference between the sheath potential within the boundary layer adjacent to the square electrode and the sheath potential within the boundary layer adjacent to the strip electrode. The difference in sheath potentials $\Delta V_s$ is included in Fig. 3.

In order to verify the foregoing points, cross-plots of the voltage drop across the load resistance against the applied voltage for three positions are given in Fig. 5. Clearly, within the experimental scatter the slopes of the curves $dV_R/dV_B$ are independent of the applied voltage $V_B$. The boundary-layer resistance is given by the relation

$$R_{BL} = R_L[(dV_B/dV_R) - 1]$$

The boundary-layer resistance is the ratio of the increment in voltage $\Delta V$ required to drive a current $I$ through the boundary layer to the current. The value of $V_B$ when $V_R = 0$, i.e., when no current flows, must equal the difference in sheath potentials between the two electrodes, $\Delta V_s$.

In Fig. 6, the measured boundary-layer resistances are plotted against position. In addition to the data obtained with a load resistance of 100 $k\Omega$, additional data obtained with a load resistance of 10 $k\Omega$ are presented. Further discussion of these results will be postponed until a theory is developed. In Fig. 7, the difference in sheath potentials $\Delta V_s$ is plotted against position. It should be emphasized that this measured sheath potential is actually the difference between the sheath potentials across the two boundary layers. The sheath potential across the boundary layer adjacent to the strip electrode is a constant, since the current always follows the same path relative to the shock front. The effect is to displace the measured sheath potential, a constant value from the sheath potential adjacent to the square electrode alone. Since the accuracy of the measurements of the sheath potential decreased as the boundary-layer resistance became large, it is difficult to determine the absolute magnitude of the sheath potential even if it is assumed that the sheath potential goes to zero as the boundary-layer resistance becomes infinite.

## III. Theory

In order to solve the problem of electrical conduction in a boundary layer, it is necessary to consider simultaneously the effects of viscosity, heat conductivity, diffusivity of the many species, and electrical conduction. Clearly, a general analytic solution to such a complex problem is not obtainable. Fortunately, it is often possible to separate the electric conduction problem from the compressible boundary-layer problem. The boundary-layer problem, including viscosity, heat conduction, and diffusion, has been solved by Fay and Riddell.[5] Numerical solutions are obtained after the partial differential equations have been reduced to total differential equations using similarity variables. A further discussion of the necessary assumptions and the limitations of the solutions is given by Lees.[6]

The problem of diffusion and electrical conduction adjacent to electrodes has been of interest in discharge tubes for some time. A considerable literature exists which is summarized by Loeb.[7] Solutions obtained are characterized by a thin region near the electrode where the electric field is appreciable and the number densities of electrons and ions are not equal. This region is generally known as a sheath. Outside the sheath, the electric field is small and the number densities of ions and electrons are nearly equal. The transport of particles under these conditions is known as ambipolar diffusion. The sheath is required because of the very different particle velocities of the ions and electrons. Without a sheath, the plasma would be depleted of electrons, and a large space charge would occur. In fact, the region in which the space charge is appreciable is the sheath.

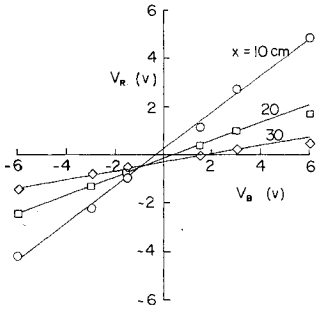


**Fig. 5 Voltage drop across the load resistor as a function of the battery voltage for several distances behind the shock wave; $R_L$ = 100 kΩ, $P_0$ = 1 mm Hg, $u_s$ = 4.35 mm/μsec, $T_0$ = 298°K.**

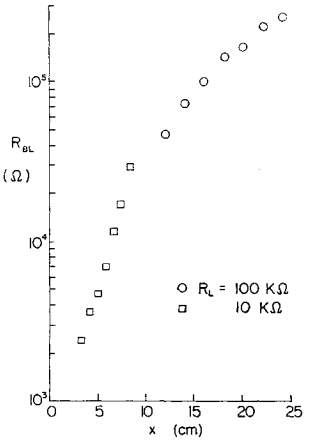


**Fig. 6 Dependence of the boundary-layer resistance on the distance behind the shock wave; $P_0$ = 1 mm Hg, $T_0$ = 298°K, $u_s$ = 4.35 mm/μsec.**

It is found that the thickness of the sheath is of the order of a debye length, $h = (\epsilon_0 kT/e^2 n_e)^{1/2}$, and in most discharge tubes this length is small compared to a mean free path, so that a collisionless sheath solution is appropriate. The collisionless sheath solution has been matched to a stagnation-point boundary-layer flow by Talbot.[8] However, in many flow problems such as the one considered in this paper, the density and degree of ionization are such that the collisionless sheath theory is not appropriate.

If the sheath thickness is large compared to the mean free path, the entire problem may be solved using continuum equations. A solution in this limit has been given by Cobine,[9] but diffusion effects were not considered. Sturtevant[10] has solved the combined diffusion-conduction equations for the time-dependent, one-dimensional initial-value problem. An analytical solution for the sphere in an infinite plasma without flow has been obtained by Su and Lam[11] in the limit of large voltage difference. Chung[12] has solved the Couette flow problem, including compressibility effects. Chung also matched his solution to a stagnation-point flow. The present authors previously presented[13] a similarity solution of the combined conduction and diffusion equations which could be matched to various external flows. This method is extended here to include compressible flows.

If the degree of ionization is low, then the presence of charged particles does not affect the solution for the velocity and temperature in a flow problem. If, in addition, the sheath thickness is small compared with the boundary-layer thickness, then convection may be neglected in solving the electrical conduction problem. As a result, the problem originally posed may be separated into two parts. The flow

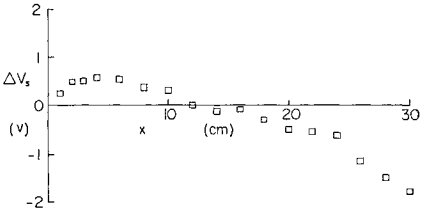


**Fig. 7 Dependence of the difference in sheath potentials on the distance behind the shock wave; $R_L$ = 100 kΩ, $P_0$ = 1 mm Hg, $u_s$ = 4.35 mm/μsec, $T_0$ = 298°K.**

problem is solved neglecting the sheath. The sheath problem is solved neglecting flow. The solutions are matched to give the complete solution. The present theory is analogous, then, to the theory of the laminar sublayer in a turbulent boundary layer where convection is also neglected.[14]

The structure of the sheath will now be determined by solving the appropriate diffusion equations along with the Poisson equation for the electric field. For the highly cooled boundary layers considered, it is appropriate to consider only laminar transport. Since the degree of ionization is very low, it is assumed that the charged particles do not affect the temperature distribution, and the transport equations can be solved independently. The equations that determine the structure of the sheath may therefore be written as[6, 10, 12]

$$nD_e(dK_e/dy) + (e/kT)D_enK_eE = -F_e \quad (1)$$

$$nD_i(dK_i/dy) - (e/kT)D_inK_iE = -F_i \quad (2)$$

$$dE/dy = (en/\epsilon_0)(K_i - K_e) \quad (3)$$

where $n$ is the number density of particles, and $K_i$ and $K_e$ are the mole fractions of ions and electrons, respectively. In writing Eqs. (1–3), it is assumed that the mobilities of the charged particles $\mu_e$ and $\mu_i$ are given by the Einstein relations:

$$\mu_e = D_ee/kT \qquad \mu_i = D_ie/kT \quad (4)$$

The ion and electron temperatures have been taken to be equal. The effect of a thermal gradient on the diffusion and on the electric field has been neglected in writing Eqs.

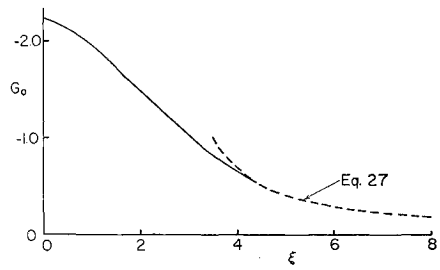


**Fig. 8 Dependence of the dimensionless electric field in the sheath on the dimensionless distance from the wall.**

(1–3). The flux of electrons $F_e$ and the flux of ions $F_i$ are constants. The difference between the ion flux and the electron flux is proportional to the electric current density,

$$j = e(F_i - F_e) \quad (5)$$

and is determined by the external circuit. The flux of ions to the wall is determined by the solution of the convective boundary-layer problem.

The binary diffusion coefficient for ions $D_i$ can be based on the neutral-neutral cross section provided that 1) ion-neutral collisions dominate the charged particle collisions, and 2) charge exchange is not important. Both of these conditions should be satisfied in the experiments considered here. The binary diffusion coefficient for electrons $D_e$ is related to the ion diffusion coefficient by $D_e/D_i = C(m_i/m_e)^{1/2}$, where the constant $C$ is of order one and depends on the relative cross sections for ion-neutral and electron-neutral collisions; the dependence on the square root of the mass ratio comes from the difference in particle velocities.

If electric conduction dominates, Eqs. (1) and (2) may be solved for the electric conduction according to

$$j = e(F_i - F_e) = (e^2/kT)D_en_eE \quad (6)$$

which is the usual form of Ohm's law, $j = \sigma E$, with

$$\sigma = (e^2/kT)D_en_e \quad (7)$$

At the other extreme, a purely diffusive solution is obtained by setting $K_e = K_i = K_a$ and assuming $F_e = O(F_i)$, with the result

$$2nD_i(dK_a/dy) = -F_i \quad (8)$$

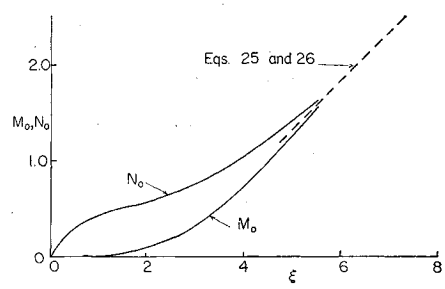


**Fig. 9 Dependence of the dimensionless number densities of ions and electrons in the sheath on the dimensionless distance from the wall.**

The solution of Eq. (8) for the case $F_e = F_i$, zero current, is known as ambipolar diffusion, where the ambipolar diffusion coefficient $D_a$ is given by $D_a = 2D_i$. It will be shown that the solution of Eqs. (1–3) with $j = 0$ asymptotically approaches ambipolar diffusion at large distances from a wall.

Appropriate boundary conditions for Eqs. (1–3) must also be specified. For a cold wall in a high density plasma, it is necessary that $K_e(0) = K_i(0) = 0$, which are the boundary conditions used in the present analysis. However, as the density of the plasma is decreased, it is expected that a jump in the number densities of charged particles at the wall may be required, just as a jump in temperature may be required at a wall in rarefied gasdynamics. The third boundary condition is used to match the asymptotic ambipolar diffusion solution. It will be seen that it is appropriate to require that $E \to 0$ as $y \to \infty$, since the plasma away from the wall cannot sustain charge separation.

To solve Eqs. (1–3), it is convenient to introduce the Howarth transformation[6] on the independent variable:

$$s = \int_0^y \frac{n}{n_w}\,dy \quad (9)$$

where the subscript $w$ refers to the value at the wall. Since it is appropriate to assume that the gas pressure is constant across the sheath, one has $n/n_w = T_w/T$. It is also a reasonable approximation to assume that

$$n^2D_e/n_w^2D_{ew} = n^2D_i/n_w^2D_{iw} = c \quad (10)$$

where $c$ is taken to be a constant. Substituting Eqs. (9) and (10) into Eqs. (1–3), one obtains

$$n_wD_{ew}\frac{dK_e}{ds} + \frac{e}{kT_w}D_{ew}n_wK_eE = -\frac{F_e}{c} \quad (11)$$

$$n_wD_{iw}\frac{dK_i}{ds} - \frac{e}{kT_w}D_{iw}n_wK_iE = -\frac{F_i}{c} \quad (12)$$

$$\frac{dE}{ds} = \frac{e}{\epsilon_0}n_w(K_i - K_e) \quad (13)$$

and it is possible to simplify the solution of Eqs. (11–13) by introducing new variables according to

$$N = \left(\frac{D_{iw}^2e^2c^2}{F_i^2\epsilon_0kT_w}\right)^{1/3}n_wK_i \qquad M = \left(\frac{D_{iw}^2e^2c^2}{F_i^2\epsilon_0kT_w}\right)^{1/3}n_wK_e$$

$$G = \frac{Ee}{kT_w}\left(-\frac{D_{iw}c\epsilon_0kT_w}{F_ie^2}\right)^{1/3} \qquad \xi = s\left(-\frac{F_ie^2}{D_{iw}c\epsilon_0kT_w}\right)^{1/3}$$

with the result

$$(dM/d\xi) + MG = \alpha \quad (14)$$

$$(dN/d\xi) - NG = 1 \quad (15)$$

$$dG/d\xi = N - M \quad (16)$$

where

$$\alpha = (1/C)(m_e/m_i)^{1/2}[1 - (j/eF_i)] \quad (17)$$

with the boundary conditions $M = N = 0$ at $\xi = 0$, and $G \to 0$ as $\xi \to \infty$. The advantage of this formulation is that there is only one variable parameter, $\alpha$.

Since Eqs. (14–16) are equivalent to a third-order nonlinear differential equation, an analytic solution cannot be expected. A numerical solution to the set of differential equations has been obtained under the limitation that the parameter $j/eF_i$ be small. That is, the flux of particles due to current flow is small compared with the flux due to diffusion. Expanding the dependent variables in powers of this parameter and keeping only the linear term, one has

$$\begin{aligned} M &= M_0 + (j/eF_i)M_1 \\ N &= N_0 + (j/eF_i)N_1 \\ G &= G_0 + (j/eF_i)G_1 \end{aligned} \tag{18}$$

Substituting Eq. (18) into Eqs. (14–16), one obtains

$$(dM_0/d\xi) + M_0G_0 = (1/C)(m_e/m_i)^{1/2} \tag{19}$$

$$(dN_0/d\xi) - N_0G_0 = 1 \tag{20}$$

$$dG_0/d\xi = N_0 - M_0 \tag{21}$$

$$(dM_1/d\xi) + M_0G_1 + G_0M_1 = (1/C)(m_e/m_i)^{1/2} \tag{22}$$

$$(dN_i/d\xi) - N_0G_1 - G_0N_1 = (1/C)(m_e/m_i)^{1/2} \tag{23}$$

$$dG_1/d\xi = N_1 - M_1 \tag{24}$$

A numerical solution of Eqs. (19–24) with $(m_i/m_e)^{1/2} = 230$ and $C = 1$ was obtained on a digital computer. The choice of mass ratio corresponds to $NO^+$, which is the principal ion in air at low temperatures. The constant $C$ is taken to be one on the basis of cross-section data given by Brown.[15] Since the cross sections are, in fact, dependent on the electric field, the assumption that $C$ is a constant is one of the limitations on the solution. The results of the computations are given in Figs. 8–11.

An asymptotic expansion of the solution of Eqs. (19–24), valid for large $\xi$, is given by

$$M_0 = \tfrac{1}{2}(\xi - \xi_0) + O(1/\xi^2) \tag{25}$$

$$N_0 = \tfrac{1}{2}(\xi - \xi_0) + O(1/\xi^2) \tag{26}$$

$$G_0 = -[1/(\xi - \xi_0)] + O(1/\xi^4) \tag{27}$$

$$M_1 = [(1/C)(m_e/m_i)^{1/2}\xi + B] + O(1/\xi^2) \tag{28}$$

$$N_1 = [(1/C)(m_e/m_i)^{1/2}\xi + B] + O(1/\xi^2) \tag{29}$$

$$G_1 = \frac{2[(1/C)(m_e/m_i)^{1/2}\xi + B]}{(\xi - \xi_0)^2} + O\left(\frac{1}{\xi^4}\right) \tag{30}$$

The asymptotic expansions are in good agreement with the computer solutions if one takes $\xi_0 = 2.4$ and $B = 0.19$. The agreement is shown in Figs. 8–11. From Eqs. (27) and (30) it is seen that the electric fields associated with both ambipolar diffusion and with current flux approach zero away from the wall. The reason for this is that the solution obtained here is for pure diffusion so that $M_0 \sim N_0 \sim \xi$ and $G_0 \sim 1/N_0 \sim 1/\xi$ with a similar argument for $G_1$.

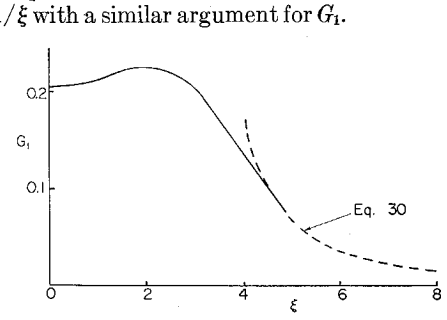


**Fig. 10 Dependence of the dimensionless electric field due to an electric current on the dimensionless distance from the wall.**

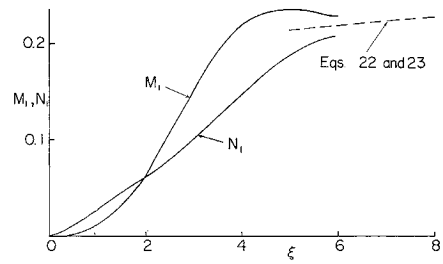


**Fig. 11 Dependence of the dimensionless number densities of ions and electrons due to an electric current on the dimensionless distance from the wall.**

If one takes $\xi = 6$ to define the edge of the sheath, then the value of the transformed independent variable at the sheath edge is given by

$$s_1 = 6\left(\frac{D_{iw}c\epsilon_0 kT_w}{-F_i e^2}\right)^{1/3} \tag{31}$$

and, in order to determine the actual sheath thickness, it is necessary to know the temperature distribution in the sheath, so that, with the requirement of constant pressure, Eq. (9) may be solved. For any sheath problem adjacent to a cold wall, Eq. (9) provides a means of calculating the sheath thickness. Clearly, a calculation based on the debye length alone is inappropriate, since no reference density $n_e$ is available on which to base the calculation. The sheath potential is related to $G_0$ as follows:

$$V_s = -\int_0^\delta E dy = -\int_0^{s_\delta} \frac{T}{T_w} E ds = \frac{-kT_w}{e}\int_0^{\xi_\delta} \frac{T}{T_w} G_0 d\xi \tag{32}$$

It should be pointed out that the foregoing integral does not converge unless the actual ambipolar diffusion problem with convection is included. The evaluation of the sheath potential is carried out in the next section. The resistance of the sheath is related to $G_1$ as follows:

$$R_s = \frac{1}{jA}\int_0^\delta E_R dy = \frac{1}{jA}\int_0^{s_\delta} \frac{T}{T_w} E_R ds = \frac{kT_w}{e^2 F_i A}\int_0^{\xi_\delta} \frac{T}{T_w} G_1 d\xi \tag{33}$$

where $A$ is the area over which current flows. Again, an actual evaluation is postponed until the next section. It should be emphasized that the resistance just obtained is valid only for small levels of the electric current. If the current flux is comparable to the diffusion flux, of charged particles, then a numerical solution of Eqs. (14–16) is required.

## IV. Comparison of Theory with Experiment

In order to discuss the experiments reported in Sec. II it is necessary to determine values of the important variables and parameters involved. The freestream and wall conditions applicable to these experiments are given in Table 1. The freestream conditions are obtained from the shock tube charts for air by Feldman.[16] The velocity $u_\infty$ is the velocity of the heated gas relative to the fixed shock wave, and $u_w$ is the velocity of the wall relative to the shock wave. The equilibrium number density of electrons $n_{e\infty}$ is based on the equilibrium equations given by Wray.[17] The mean free paths $\lambda$ are based on the neutral-neutral mean free path for $N_2$. The ionization relaxation time $\tau_e$ is obtained from the data of Lin.[18] The debye lengths $d$ are based on the freestream number density of electrons, since it is the only finite reference value available. Since the sheath is clearly much thicker than the wall debye length, a continuum analysis is appropriate for the experiments considered here.

**Table 1 Summary of experimental conditions**

| | Freestream | Wall |
|---|---|---|
| Pressure, mm Hg | 202 | 202 |
| Temperature, °K | 4560 | 298 |
| Density, atm | 0.0173 | 0.265 |
| Velocity, cm/sec | $0.38 \times 10^5$ | $4.35 \times 10^5$ |
| Total enthalpy, cm²/sec² | $9.18 \times 10^{10}$ | $9.45 \times 10^{10}$ |
| Electron density, electrons/cm³ | $1.235 \times 10^{13}$ | ~0 |
| Ionization relaxation time, sec | $1.24 \times 10^{-5}$ | ... |
| Mean free path, cm | $4.33 \times 10^{-4}$ | $2.83 \times 10^{-5}$ |
| Debye length, cm | $1.32 \times 10^{-4}$ | $3.40 \times 10^{-5}$ |

The theory developed in the previous section will be applied now. It will be assumed that it is appropriate to separate the sheath problem from the compressible wall boundary-layer problem. The equations governing the wall boundary layers in a shock tube are identical to those for a flat-plate boundary layer. However, the boundary conditions differ in steady-state, shock-fixed coordinates. Solutions for shock-tube boundary layers without chemical reactions have been given by Mirels.[19] Under the conditions considered here, the only chemical reaction that appreciably affects the enthalpy of the gas is the dissociation of oxygen. From Table 1, it is seen that the total enthalpy at the wall, $h_{0w}$, is approximately equal to the total enthalpy in the freestream, $h_{0\infty}$. It has been shown by many authors[6] that, if the boundary conditions on the total enthalpy are the same and if the Prandtl and Lewis numbers are near one, it is a good approximation to assume that the total enthalpy is constant throughout the boundary layer. Therefore, it is assumed that $h_0 - h_w = 9.45 \times 10^{10}$ cm²/sec². For the region near the wall where the concentration of atomic oxygen is small, the temperature can be obtained from the usual equation for the total enthalpy:

$$h_0 - h_w = \tfrac{1}{2}u^2 + c_p(T - T_w) \tag{34}$$

if the velocity is known. Introducing an assumption on the product of the density and the viscosity, the velocity profile in the boundary layer does not depend on chemistry. Introducing the usual dimensionless variables,[6]

$$\eta = \left(\frac{\rho_\infty u_\infty}{2\mu_\infty x}\right)^{1/2} \int_0^y \frac{\rho}{\rho_\infty}\, dy \qquad f_\eta = \frac{u}{u_\infty}$$

the momentum and continuity equations can be considered to give

$$\left(\frac{\rho\mu}{\rho_\infty\mu_\infty} f_{\eta\eta}\right)_\eta + f f_{\eta\eta} = 0 \tag{35}$$

and the appropriate boundary conditions are

$$\text{at } \eta = 0: \quad f = 0,\ f_\eta = 11.45$$

$$\text{as } \eta \to \infty: \quad f_\eta \to 1$$

Assuming a linear variation of the $\rho\mu$ ratio, an approximate solution for the velocity profile is found using momentum methods.[20] The fifth-order polynomial for $f$ which was obtained can be written

$$f = 11.45\eta - 6.16\eta^2 - 0.874\eta^3 + 1.88\eta^4 - 0.455\eta^5 \tag{36}$$

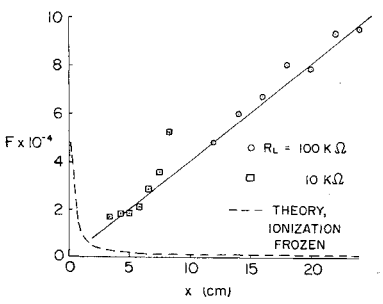


**Fig. 12 Dependence of the dimensionless boundary-layer resistance on the distance behind the shock wave; $P_0$ = 1 mm Hg, $u_s$ = 4.35 mm/μsec, $T_0$ = 298°K.**

It will be seen that the important contributions to the resistance and sheath potential are from the region adjacent to the wall. Therefore, it is appropriate to use Eq. (34) to determine the temperature. It is also consistent to use an approximate expression for the temperature valid near the wall. Keeping only the first four terms in powers of $\eta$, the temperature may be written

$$T/T_w = 1 + 68.4\eta - 22.3\eta^2 - 57.3\eta^3 + 55.8\eta^4 \tag{37}$$

With this expression for the temperature, the integrals for the sheath potential and boundary-layer resistance given in Sec. III can be evaluated now.

First, the sheath potential from Eq. (32) will be determined. It is convenient to break the integral in Eq. (32) into two parts. In the interval near the wall $0 < \xi < 6$, the dependence of $G_0$ on $\xi$ given in Fig. 9 is used. In this interval, a linear expression for the temperature is used and is written in terms of $\xi$:

$$T/T_w = 1 + 68.4\eta = 1 + 11.4\eta_s\xi \tag{38}$$

where

$$\eta_s = 6\,\frac{\rho_w}{\rho_\infty}\left(\frac{\rho_\infty u_\infty}{2\mu_\infty x}\right)^{1/2}\left(-\frac{D_{iw}c\epsilon_0 kT_w}{F_i e^2}\right)^{1/3} \tag{39}$$

and $\eta_s$ is the value of $\eta$ corresponding to $\xi = 6$, i.e., the edge of the sheath. The inner contribution to the sheath potential is given by

$$\int_0^6 \frac{T}{T_w} G_0 d\xi = -6.73 - 153.7\eta_s \tag{40}$$

and it is seen that the variation of temperature in the sheath has a strong influence. Turning to the outer contribution to the integral in Eq. (32), the asymptotic expression for $G_0$ given in Eq. (27) is used. Using the temperature ratio as given in Eq. (37), the outer contribution to the integral is

$$\int_6^{\xi_\delta} \frac{T}{T_w} G_0 d\xi = -62.3 + \ln\eta_s - 57.5\eta_s + 27.3\eta_s \ln\eta_s - 2.6\eta_s^2 + 30.5\eta_s^3 - 21.5\eta_s^4 \tag{41}$$

As long as $\eta_s < 0.5$, the convergence of the forementioned series in $\eta_s$ is good, and the approximate expression for the temperature ratio given in Eq. (37) is adequate. It should be emphasized that the outer integral, the contribution outside the sheath, makes a significant contribution to the sheath potential. Combining Eqs. (40) and (41), the dimensionless sheath potential is given by

$$V_s e/kT_w = 70.0 - \ln\eta_s + 211.2\eta_s - 27.3\eta_s \ln\eta_s + 2.6\eta_s^2 - 30.5\eta_s^3 + 21.5\eta_s^4 \tag{42}$$

and this expression should be valid as long as $\eta_s < 0.5$.

Using the same method of splitting the required integral, the boundary-layer resistance is obtained from Eq. (33). Using the sheath thickness $\eta_s$ as the independent variable, it is natural to introduce a dimensionless boundary-layer resistance $F$ according to

$$F = \epsilon_0 c D_{iw} RA \left(\frac{\rho_w}{\rho_\infty}\right)^3 \left(\frac{u_\infty \rho_\infty}{2\mu_\infty x}\right)^{3/2} \tag{43}$$

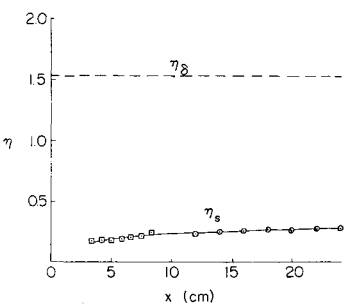


**Fig. 13 Dependence of the dimensionless, transformed sheath thickness on the distance behind the shock wave; $P_0$ = 1 mm Hg, $u_s$ = 4.35 mm/μsec, $T_0$ = 298°K.**

Using a linear temperature profile as just mentioned, along with the numerical values of $G_1$ given in Fig. 11 for the inner contribution, and the asymptotic expression for $G_1$ given in Eq. (30), along with the temperature as given in Eq. (38) for the outer contribution, the dependence of $F$ on $\eta_s$ is found to be

$$F = (\eta_s^3/216)(1.155 - 0.0087 \ln\eta_s + 25.0\eta_s - 3.85\eta_s \ln\eta_s + 1.16\eta_s^2 - 1.78\eta_s + 1.17\eta_s^4) \quad (44)$$

Again the solution is valid as long as $\eta_s < 0.5$.

In principle, it is now possible to determine $\eta_s$ as a function of $x$ from Eq. (39), to plot $V_s e/kT_w$ and $F$ as functions of $x$ from Eqs. (42) and (44), and then to compare the results with the experimental values given in Sec. II. However, in order to determine $\eta_s$ as a function of $x$, one must know $F_i$ as a function of $x$. This requires a solution of the ambipolar diffusion problem in the compressible boundary layer. Such a solution is relatively straightforward if the ionization reaction is frozen, that is, if no appreciable recombination of ions and electrons takes place in the boundary layer. A solution can also be obtained if it is assumed that the ion and electron concentrations are in thermal equilibrium throughout the boundary layer. However, the latter solution would lead to an infinite boundary-layer resistance for the wall temperatures considered here and is clearly not appropriate. Unfortunately, a solution of the boundary-layer diffusion problem with finite recombination rates for the ionization reaction is beyond the scope of the present investigation. Therefore, this comparison must be restricted to the case of frozen flow.

Before any comparison between the theoretical and experimental values of the dimensionless resistance is made, it should be emphasized that it is not expected that the theory is applicable to the full range of applied voltages considered in the experiments. Since it is required that $j \ll eF_i$ in the theory, the theory is expected to be applicable only in the range $V_B \ll V_s$. However, since the experiments indicate a resistance that is independent of the current level within the range of battery voltages considered, a comparison of the measured values with the linearized theory would seem reasonable.

In Fig. 12, the dependence of $F$ on $x$ for frozen flow obtained from Eq. (44) is compared with the experimental values from Fig. 6. It is concluded that recombination plays an important role in the problem, since the experimental values of the resistance are as much as an order of magnitude larger than the theoretical values based on frozen flow. Such a result is hardly unexpected, since considerable recombination should occur in the outer portion of the boundary layer before the ionization recombination reaction freezes. Also, if the flow is frozen it can be shown that the external resistance is greater than the boundary-layer resistance, since the measured resistance is strongly dependent on $x$ the boundary-layer resistance must dominate and considerable recombination must occur.

In order to investigate the validity of the theory, the sheath thicknesses corresponding to the measured boundary-layer resistances are obtained from Eq. (44) and are plotted against $x$ in Fig. 13. The boundary-layer thickness is also included. Certainly a continuum theory for the structure of the sheath is appropriate. Also, the sheath is sufficiently thin compared to the boundary layer so that the approximation of dropping convective terms in the sheath solution should be valid.

In Fig. 14 the dimensionless sheath potential $V_s e/kT_w$ for frozen flow from Eq. (42), is compared with the experimental values. Two volts have been added to the experimental results as given in Fig. 7 as a reasonable value for the reference potential. Also included in Fig. 14 are the values of the sheath potential corresponding to the linear correlation

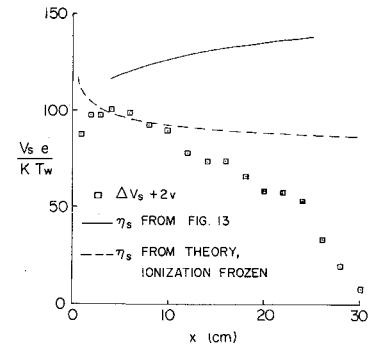


**Fig. 14 Dependence of the dimensionless sheath potential on the distance behind the shock wave; $P_0 = 1$ mm Hg, $u_s = 4.35$ mm/$\mu$sec, $T_0 = 298°$K.**

of the data in Fig. 12. It is seen that the predicted magnitude of the sheath potential is in good agreement with experiment. However, the dpendence on $x$ is not particularly good. The reason for this discrepancy is not clear.

## References


[1] Brogan, T. R., "The conduction of electric current to cold electrodes in shock tubes," Thesis, Cornell Univ., Ithaca, N. Y. (1956).

[2] Pain, H. J. and Smy, P. R., "Experiments on power generation from a moving plasma," J. Fluid Mech. **10**, 51–64 (1951).

[3] George, D. W. and Messerle, H. K., "Electrode conduction processes in air plasmas," J. Fluid Mech. **13**, 465–477 (1962).

[4] Jukes, J., "Heat transfer from highly ionized argon produced by shock waves," Thesis, Cornell Univ., Ithaca, N. Y. (1956).

[5] Fay, J. A. and Riddell, F. R., "Theory of stagnation point heat transfer in dissociated air," J. Aeronaut. Sci. **25**, 73–85 (1958).

[6] Lees, L., "Convective heat transfer with mass addition and chemical reactions," *Third AGARD Colloquium: Combustion and Propulsion* (Pergamon Press, London, 1958), pp. 451–498.

[7] Loeb, L. B., *Basic Processes in Gaseous Electronics* (University of California Press, Berkeley, Calif., 1955), pp. 329–373.

[8] Talbot, L., "Theory of the stagnation-point langmuir probe," Phys. Fluids **3**, 289–298 (1960).

[9] Cobine, J. O., *Gaseous Conductors* (McGraw-Hill Book Co., Inc., New York, 1941), pp. 128–129.

[10] Sturtevant, B., "Diffusion in a slightly ionized gas with application to effusion from a shock tube," Phys. Fluids **4**, 1064–1073 (1961).

[11] Su, C. H. and Lam, S. H., "The continuum theory of spherical electrostatic probes," Rept. 605, Dept. Aeronaut. Eng., Princeton Univ., Princeton, N. J. (1962).

[12] Chung, P. M., "Electrical characteristics of couette and stagnation boundary layer flows of weakly ionized gases," Rept. TDR-169(3230-12) TN-2, Aerospace Corp., Inglewood, Calif. (1962).

[13] Turcotte, D. L. and Gillespie, J., "Boundary layer resistance and the sheath potential in a shock tube," ARS Preprint 2634-62 (1962).

[14] Turcotte, D. L., "A sublayer theory for fluid injection into the incompressible turbulent boundary layer," J. Aerospace Sci. **27**, 675–679 (1960).

[15] Brown, S. C., *Basic Data of Plasma Physics* (Technology Press and John Wiley and Sons Inc., New York, 1959), pp. 47–98.

[16] Feldman, S., "Hypersonic gas dynamic-charts for equilibrium air," Res. Rept. 40, Avco-Everett Res. Lab., Everett, Mass. (1957).

[17] Wray, K. L., "Chemical kinetics of high temperature air," *Hypersonic Flow Research* (Academic Press, New York, 1962), pp. 181–204.

[18] Lin, S. C., "Ionization phenomena of shock waves in oxygen-nitrogen mixtures," Avco-Everett Res. Lab., Res. Rept. 33 (1958).

[19] Mirels, H., "Laminar boundary layer behind shock advancing into stationary fluid," NACA TN 3401 (1955).

[20] Schlichting, H., *Boundary Layer Theory* (McGraw-Hill Book Co., Inc., New York, 1955), pp. 201–206.